Search for tumor-specific frequencies of amplitude-modulated 27 MHz electromagnetic fields in mice with hepatocarcinoma xenografted tumors

Bernard Veyret, Delia Arnaud-Cormos, Emmanuelle Poque, Florence Poulletier de Gannes, Annabelle Hurtier, Rodolphe Decourt, Sokha Khiev, Gilles N'kaoua, Isabelle Lagroye, Philippe Lévêque, et al.

International Journal of Radiation Biology

Search for Tumor-Specific Frequencies of Amplitude-Modulated 27 MHz Electromagnetic Fields in Mice with Hepatocarcinoma Xenografted Tumors

Bernard Veyret [1], Delia Arnaud-Cormos [2], Emmanuelle Poque [1], Florence Poulletier de Gannes [1], Annabelle Hurtier [1], Rodolphe Decourt [3], Sokha Khiev [4], Gilles N'Kaoua [1], Isabelle Lagroye [1,5], Philippe Lévêque [2] and Yann Percherancier *[1]

[1] Université de Bordeaux, CNRS, IMS laboratory, UMR5218, F-33400 Talence, France

[2] Université de Limoges, CNRS, XLIM, UMR 7252, F-87000 Limoges, France

[3] Université de Bordeaux, CNRS, ICMCB, UMR 5026, F-33600 Pessac, France

[4] Université de Bordeaux, CNRS, LCPO, UMR 5629, F-33600 Pessac, France

[5] Paris Sciences et Lettres Research University, F-75006 Paris, France

*Author correspondence (YP): yann.percherancier@ims-bordeaux.fr

BV: bernard.veyret@ims-bordeaux.fr; DAC: delia.arnaud-cormos@xlim.fr,

EP: emmanuelle.poque@ims-bordeaux.fr; FPDG: florence.poulletier@ims-bordeaux.fr;

AH: annabelle.hurtier@bordeaux-inp.fr; RD: decourt@icmcb-bordeaux.cnrs.fr;

SK: Sokha.Khiev@enscbp.fr; GNK: gilles.nkaoua@ims-bordeaux.fr;

IL:isabelle.lagroye@ims-bordeaux.fr; PL: philippe.leveque@unilim.fr

Abstract

Aim: The Pasche research group has reported that tumor-specific electromagnetic field frequencies have physiological and potential anti-tumor effects in cells, animals, and humans. Our aim was to investigate whether these fields have similar effects on physiological parameters in murine tumor models.

Methods: Human HuH7 or HEPG2 cells were implanted in the right flank of 8-week-old female RAG gamma 2C immunodeficient mice. An oximeter was used to record systolic blood pressure (pulse) in free-roaming conscious mice. Mice pulses were recorded and analyzed using a in-house software that also controlled the low-frequency generator for modulating the 27.12 MHz carrier wave at selected frequencies.

Results: We performed exposures using both systematic scans at low-frequencies and at the pre-determined frequencies reported by the Pasche group as altering both pulse and tumor growth in humans. Those exposures produced no detectable change in physiological parameters of tumor-bearing mice.

Conclusion: No tumor-related frequencies were found, neither using systematic scans of frequencies nor published specific frequencies. There might obviously be differences between animal and human models, but our approach did not confirm the physiological data of the human Pasche group data.

Keywords: electromagnetic fields – xenograft tumor – tumor-specific frequencies

1. Introduction

The Pasche group has reported evidence that radiofrequency electromagnetic fields, amplitude-modulated at discrete frequencies (AM-RF), elicited therapeutic responses in patients with tumors (Barbault et al. 2009; Costa et al. 2011; Zimmerman et al. 2012). Using a patient-based biofeedback approach, these authors identified several series of discrete frequencies that were specific of tumor types, based on the monitoring of radial pulse in patients (Barbault et al. 2009). Their clinical results provided evidence that intrabuccal exposure with AM-RF at tumor-specific frequencies was well tolerated and led to long-lasting therapeutic responses in patients with advanced cancer (Costa et al. 2011; Sharma et al. 2019). They also reported that cancer cell proliferation was altered *in vitro* using the same tumor-specific AM-RF, which had been identified in patients diagnosed with cancer (Zimmerman et al. 2012; Sharma et al. 2019; Jimenez et al. 2019). They reported that tumor-specific AM-RF blocked the growth of cancer cells, modified gene expression, and disrupted mitotic spindle. In their most recent reports, they identified Ca^{2+} influx through $Ca_v3{\cdot}2$ T-type voltage calcium channels as the key event in both AM-RF antiproliferative effects and down-regulation of cancer cells, which likely correlate with the long-term responses observed in patients with advanced cancer (Sharma et al. 2019; Jimenez et al. 2019).

However, on the basis of the aforementioned published studies, one can identify gaps in knowledge that hinder the acceptance of this cancer treatment (Blackman. 2012). In particular, one may wonder how the reported biofeedback endpoints (pulse amplitude and blood pressure) are related to the disease and to the effective frequencies to treat patients. Moreover, how AM-RF exposure specifically affect tumor cells *in vitro* is still a pending question.

In this work, we implemented a complementary approach using a mouse tumor model in the search for frequency specific effects on physiological parameters. This was done in

order to facilitate further mechanistic research in animals. The Pasche group reported that specific AM-RF, initially identified in human patient with hepatocellular carcinoma (HCC), inhibits the growth of HEPG2 and HuH7 HCC cells *in vitro* (Zimmerman et al. 2012). We thus used RAG gamma 2C immunodeficient mice xenografted with human HuH7 or HEPG2 HCC cells and searched for specific AM-RF effects on physiological parameters. We report here the use of such previously published AM frequencies, active on both pulse and tumor growth (Barbault et al. 2009; Costa et al. 2011; Zimmerman et al. 2012), as well as systematic scanning of amplitude-modulation (AM) frequencies. These exposures did not produce any detectable change in physiological parameters on freely-roaming mice.

2. Material and Methods

2.1. Tumor model, mice housing, anesthesia, and ethical issues

Human HuH7 and HepG2 cell lines were used as representative HCC cells as indicated in (Zimmerman et al. 2012) and were kindly provided by J. Rosenbaum (INSERM U889, Bordeaux University, Bordeaux, France). Cells were maintained in Dulbecco's modified Eagle's medium high glucose (Cat. No. D6429; Sigma-Aldrich, St. Louis, MO) supplemented with 10% fetal bovine serum, 100 U/ml penicillin and streptomycin.

Immunodeficient RAG-2/γ(c)KO mice were produced, housed, and xenografted in the animal facility of Bordeaux University (agreement N°C33-522-2). Xenograft tumors were obtained by subcutaneous injection of one million cells into the right flank of 8-week-old female RAG-2/γ(c)KO mice. Tumor size measurements were initiated 8 days post inoculation and monitored three times per week. Tumor volume (in mm^3) were evaluated using calipers using the following formula: length x $width^2/2$. When tumors became palpable, the mice were transferred to the IMS laboratory animal facility (agreement N°A33-522-5) for RF exposure. Both animal facilities adhere to the 3R principles of Replace, Refine and Reduce, and follows

the EC policy on animal research (European Directive UE/2010/63). In both animal facilities, animals were housed under the following environmental conditions: 12h dark–12h light cycle, temperature 21 ± 1 °C, humidity 55–65%. They were fed *ad libitum* with food pellets (Standard Diet A04, SAFE, France) and water. On arrival to the IMS laboratory facility, animals were housed for one week prior to the start of RF exposure experiments.

A total of 19 mice were used for analysis: 6 were xenografted with HEPG2 cells, 6 with HuH7 cells, and 7 healthy mice were used as control. For each experimental and sham group, relevant characteristics and health status of animals was recorded during the study. Mice were sacrificed when the tumor volume reached 1000 mm^3. When indicated, mice pulse pleth was recorded under anesthesia following intramuscular injection of ketamine (100 mg/kg, Vibrac, Carros, France) and xylazine (10 mg/kg, Vibrac, Carros, France). Dobutamine (10 µg/kg, PanPharma, Luitré, France) was intraperitoneally injected in anesthetized mouse. Maximal exposure duration was 1 h per day and 5 days per week. Animals were exposed randomly between 9:00 a.m. and 5:00 p.m. After the last exposure, animals were sacrificed by cervical dislocation. All animal procedures were done according to the institutional guidelines and approved by the local ethics committee (CEEA50) and local veterinary authority in Bordeaux (agreement number: 05107.03).

2.2. Pulse oximetry measurements

Mice plethysmographic waveforms were recorded in 1-s blocks using a MouseOx pulse oximeter (STARR Life Sciences, Oakmont, PA, USA), the CollarClip™ sensor of which was placed on the shaved skin on the mice neck. Using the LabView programming language (National Instruments, Austin, TX, USA), an in-house software was developed to acquire and analyze the raw pulse signals recorded from the analog output of the MouseOx pulse oximeter

through a data acquisition card (NI SCC 68, National Instruments, Austin, TX, USA). A schematic of the whole system is given in Fig. 1.

2.3. Exposure system driving, and pulse signal rejection criteria

Mice plethysmographic waveforms were recorded on freely-moving awake mice fitted with a pulse oximeter CollarClip^{TM} sensor and exposed to AM-RF. Mice were first accustomed in the dark inside a 25 x 25 cm black cardboard box for 30 minutes before RF exposure and pulse monitoring. Two-Hz increments in modulation frequency were then applied sequentially during 4 s. They consisted in either HCC-specific modulation frequencies previously reported (Costa et al. 2011; Zimmerman et al. 2012) or modulation frequencies scanned in the ranges indicated in Table 1. Since the MouseOx analog pulse signal was subject to alteration caused by mice movements (Supplementary Fig. 1), both mice motion and pulse pleth errors along with the mice plethysmographic waveforms were recorded in real time via the data acquisition card and Labview interface. Mice motion and movement were monitored using a piezoelectric pressure sensor placed underneath the cardboard box. Pulse pleth errors from the MouseOx pulse oximeter were monitored using a Starr-Link analog data output module (STARR Life Sciences). When mouse movement or pulse pleth error were detected, the session was cancelled and both AM RF exposure and pulse pleth recording were halted until the rejection criteria disappeared. Then, the 4-s recording session resumed at the last tested modulation frequency.

2.4. Exposure system

The exposure setup was composed of a low-frequency signal generator (33120A, Agilent, Santa Clara, CA, USA) modulating a high-frequency signal generator (SML02, Rohde & Schwarz, Munich, Germany) emitting a 27.12 MHz carrier signal, a directional

coupler which allowed forward and reflected signal measurements, and a 50 Ω impedance matching device maximizing power transfer into the sample through a disposable electrode stuck to the mouse shaved neck (Fig.1 and Fig. 2a). The specific absorption rate (SAR) in the whole body of the sample was assessed at 27 MHz. Numerical dosimetry of a complex and realistic animal model was carried out using an in-house electromagnetic software based on the Finite Difference-Time Domain method (FDTD) (Yee. 1966; Leveque et al. 1992; Taflove & Hagness, 2005). The electrode-based delivery system was composed of a coaxial cable with inner and outer conductors connected to the exposed sample and to the ground plane, respectively (Fig. 2b). A versatile wire was modeled with an arbitrary chosen geometry between the BNC connector and the electrode placed on the exposed sample, which was separated from the ground plane by a plastic layer. During simulation, all metallic parts were considered as perfect electric conductors and the dielectric materials were modeled with their electromagnetic properties, i.e. relative permittivity and electrical conductivity. The 20 g mouse was modeled with the properties of 36 different tissues extracted at 27 MHz from (Gabriel et al. 1996) [http://niremf.ifac.cnr.it/docs/DIELECTRIC/home.html]. The mouse model consists in an extrapolation of a 0.75 mm mesh size rat model (Brooks AFB, San Antonio, TX). This rat model had been used in several previous studies (Poulletier de Gannes et al. 2009; Grigoriev et al. 2010; Wu et al. 2010; Collin et al. 2016). The permittivity of the 1 mm plastic layer underneath the mouse was set to 2.5. The numerical volume was meshed with a uniform 0.33 x 0.33 x 0.33 mm mesh grid. The simulated volume was limited using perfectly matched layers, directly integrated into the code (Berenger. 1994). A 0.385 ps time resolution and 120,000 time steps for a total of 46 ns were used in the FDTD simulation. For validation and comparison with measurements, a simple homogenous model (plastic dish filled with 20 g tissue-equivalent liquid) was studied (data not shown).

The SAR values were assessed from the electric field simulations as:

$$SAR = \frac{\sigma E^2}{2\rho} \text{ (W/kg)} \quad (1)$$

where E is the electric field (V/m), ρ is the biological sample density (kg/m^3) and σ is the electrical conductivity (S/m). To assess the impedance matching between the generator and the delivery system, input impedance and reflection coefficient evaluation was carried out.

2.5. Impedance matching and SAR assessment at 27 MHz

For the assessment of impedance matching between the generator and the delivery system, S_{11} reflection coefficient simulation and measurement were performed. Without the matching device, the delivery system had an impedance equivalent to a 17.8 pF electrical capacitor. By inserting the impedance matching device and adjusting the capacitors with the following values C1=47.8 pF, C2=179 pF, a –20 dB reflection coefficient was obtained at 27 MHz (Fig. 3a). Fig. 3b shows the spatial SAR distribution computed at 27 MHz. In the modeled mouse, the whole-volume SAR value was 40.7 W/kg at 1 W incident power. The higher SAR values were localized in the vicinity of the electrode and decreased rapidly with the distance from the electrode. For a 1 W incident power, the brain-averaged SAR was 1.6 W/kg with a standard deviation of 1.2 W/kg.

3. Results

3.1. Positive controls

We first tested whether our experimental setup, described in Fig. 1, allowed the detection of modifications in mice pulse pleth signal. The pulse oximetry signal in an anesthetized RAG-2/γ(c)KO mouse was recorded before and after IP injection of Dobutamine, a well-known catecholamine derivative developed as a cardiotonic agent (Tuttle & Mills. 1975). As shown in Fig. 4, IP injection of dobutamine induced a progressive increase in both pulse rate and pulse amplitude that was efficiently monitored in real time. This

validated our experimental procedure to assess the potential effect of AM-RF on mouse pulse signal.

3.2. Monitoring mouse pulses under AM-RF exposure

Recording of the potential effects of amplitude-modulated frequencies on the pulses of xenografted mice started as soon as the tumor volume reached 36 mm^3 and was performed several times at different phases of tumor growth, until the tumor volume reached 1000 mm^3. Two exposure protocols were used while searching for biologically active AM-RF (see below and Table 1).

3.3. Scanning using "human patient" frequencies

We first tested whether the HCC-specific modulation frequencies detected on human cancer patients based on the increase in their pulse amplitude (Barbault et al. 2009) increased HCC-xenografted mouse pulse amplitude. RAG-2/γ(c)KO mice bearing HuH7 or HEPG2 xenograft of various volumes (see table 1) were sham-exposed (27.12 MHz carrier wave only) or exposed to the HCC-specific modulation frequencies while the pulse pleth signal was acquired and pulse rate and amplitude analyzed in real time. Each recording session started and ended with a sham exposure and the HCC-specific modulation frequencies were applied in between these sham exposure sequences. Two series of 30-40 AM frequencies selected from the list of HCC-specific modulation frequencies reported by the Pasche group were tested: from 410 Hz to 2419 Hz and from 4289 Hz to 6733 Hz (Costa et al. 2011; Zimmerman et al. 2012) (Table 1). Each frequency was applied during 4 s with an incident power of 13.5 dBm corresponding to a whole-body SAR of 0.9 W/kg. A total of 22 recording sessions where performed using two different sets of HCC-specific modulation frequencies, two different HCC xenografted mouse models and various tumor volumes up to 1000 mm^3.

As illustrated in Fig. 5, we observed only rare and stochastic transient increases or decreases in pulse amplitude or frequency. Under exposure to HCC-specific modulation frequencies, no sustained and reproducible increases in either mice pulse amplitude or pulse rate were observed.

3.4. Systematic scanning for mouse-specific modulation frequencies on HCC tumor-bearing mice

As specific frequencies determined on human patients were ineffective on xenografted mice, one might conclude that mouse-specific frequencies are different from the human ones. We therefore scanned various ranges of AM frequencies to seek for reproducible effects of one or more specific AM frequencies on HCC xenografted mice. As previously indicated, this study was performed on RAG-2/γ(c)KO mice bearing HuH7 or HEPG2 xenograft of various volumes (see table 1). We performed a systematic frequency scanning over ranges of 400 to 500 Hz starting at frequencies such as 1 Hz, 2.3 kHz, 4 kHz, 10 kHz and 100 kHz. Frequency ranges were scanned by steps of 2 Hz, each exposure phase lasting 4 s. As exemplified in Fig. 6A, focusing on mice pulse amplitude measured under exposure to AM frequencies between 2300 and 2700 Hz, we observed only rare and stochastic transient increase in mice pulse pleth amplitude. Similar results were also found during sham-exposure (Fig. 6B). In conclusion, no mouse-specific AM frequencies were detected that produced an increase in mouse pulse pleth amplitude.

3.5. Peak-to-peak analysis of the mice pulse pleth signals

According to the report by Barbault et al. (2009) (Barbault et al. 2009), tumor specific AM frequencies produced an increase in the amplitude of the radial pulse for one or more beats over a typical recording period of 3 s for each AM frequency tested. Our analysis was based on the detection of changes in average amplitude or frequency of pulses over one-

second blocks recorded for four seconds for each AM-frequency tested. Since the normal pulse rate of mice lies between 8 and 10 Hz, effects on single beats may have been missed. We therefore analyzed our data using a peak-to-peak analysis of the recorded pulse waveforms obtained in mice exposed to AM-RF (Fig. 7). For each AM frequency tested, we calculated $\bar{X}$, the average amplitude of the mice pulses over the 4 s recording period, along with the related standard deviation (σ), and then calculated the percentage of beats for which the peak-to-peak amplitude or frequency exceeded $\bar{X}+2\sigma$ (Fig. 7A). Under exposure between 2300 and 2700 Hz AM-RF, we found that, on average, over all experimental conditions tested as functions of tumor size and xenograft type, less than 3% of the beats were "out of range" (Fig. 7B). Moreover, this percentage was similar under sham- and real-exposure conditions indicating that none of the tested AM frequencies modified the amplitude of the mice beats.

4. Discussion

In this work, we searched for alterations in pulse amplitude or frequency in mice under exposure to AM-RF, in line with the findings of the Pasche group on human subjects. We found no evidence of such effects on the pulse, but did not test the effects of such exposures on the growth of tumors. The Pasche group reported effects of AM-RF exposure on tumor growth in mice but did not look for effects on the pulse parameters in the exposed mice (Jimenez et al. 2019; Sharma et al. 2019). As described by Jimenez et al. (Jimenez et al. 2019), HCC cells were injected subcutaneously in NOD SCID mice exposed to HCC-specific AM-RF at a specific absorption rate of 67 mW/kg, while we used 900 mW/kg in our study. The selected frequencies were the ones determined in human-based pulse changes. While HCC xenografts grew in control mice, there was significant tumor shrinkage in mice exposed to HCC-specific modulation frequencies and residual xenograft tumor cells were infiltrated with fibrous tissue. A discrepancy thus exists between the above data on tumor growth in

mice under AM-FR exposure and the absence of effects on pulse in mice exposed to the same frequencies in our work. Animal tumor models and exposure characteristics were similar in the two laboratories except that a whole-body setup was used for mice exposure by the Pasche group (Capstick et al. 2016).

Initial experimental work by the Pasche group dealt with human subjects (Barbault et al. 2009; Costa et al. 2011). In these former works, effects were found using AM-RF exposure at selected frequencies on cancer bearing patients and some *in-vitro* evidence regarding the mechanisms of the effects was reported (Zimmerman et al. 2012; Zimmerman et al. 2013; Jimenez et al. 2019; Sharma et al. 2019). However, there has been no independent replication of any of these studies. Ours was the first to address the very existence of frequencies linked with alterations of physiological parameters in mice, but it did not aim at exploring the effects on tumor growth in the same mice.

Further investigations should be carried out to complete the assessment of both the effects on physiological parameters and tumor growth *in vivo* and effects on cells in culture. Potential mechanisms linking the two types of AM-RF effects are still unknown. Moreover, the link between development of tumors and pulse changes in human and animal models also needs to be elucidated. These studies will help foster the development of new therapeutic approaches using RF exposure as suggested recently (Jimenez et al. 2018).

In conclusion, we did not provide evidence that RF exposure alters biopotential in tumor-bearing mice, in contrast to the findings of the Pasche group in humans. There might obviously be differences between the animal and human models, but our approach did not confirm the data of the Pasche group on animal and human models. However, our experimental approach is well suited to test other animal models and hypotheses using our ready-to-use exposure system.

Abbreviation

AM-RF: amplitude-modulated radiofrequency fields

HCC: hepatocellular carcinoma

SAR: specific absorption rate

FDTD: Finite Difference-Time Domain method

BNC: Bayonet Neill–Concelman *connector*

Acknowledgements

The authors would like to thank Antonio Šarolić, FESB, University of Split, Croatia, and Michal Teplan, Institute of Measurement Science, Slovak Academy of Sciences, Bratislava, Slovakia, for providing insightful comments and reviewing the manuscript. Neither of them received any compensation for their work. Oral presentation: 2014 Annual Meeting of the Bioelectromagnetics Society, Cap Town, South Africa; COST EMF-MED Workshops and Meetings: 14-16 February 2017 – Warsaw, Poland.

Funding source

The costs associated with the design and engineering of the devices used in this study were paid by YP, PL, IL, and BV using recurrent research teams funding. This study was performed within the framework of COST action EMF-MED (BM1309) supported by COST (European Cooperation in Science and Technology).

Declaration of interest

The authors declare no competing interests.

Authors' contributions

YP and BV conceived and designed the study. PL and DAC designed the device and performed the electromagnetic dosimetry. YP collected and assembled the data. YP, RD, SK and GNK programmed the LabView interface for the acquisition and analysis of oximetry. AH, EP and FPDG took care of the animals. YP, BV, IL, DAC and PL wrote the manuscript. All co-authors read and approved the final manuscript.

References

Barbault A, Costa FP, Bottger B, Munden RF, Bomholt F, Kuster N, Pasche B. 2009. Amplitude-modulated electromagnetic fields for the treatment of cancer: discovery of tumor-specific frequencies and assessment of a novel therapeutic approach. J Exp Clin Cancer Res. 28: 51.

Berenger J-P.1994. A Perfectly Matched Layer for the Absorption of Electromagnetic Waves J. Comput. Phys.. 114: 185-200.

Blackman CF.2012. Treating cancer with amplitude-modulated electromagnetic fields: a potential paradigm shift, again? Br J Cancer. 106: 241-242.

Capstick M, Gong Y, Pasche B, Kuster N. 2016. An HF exposure system for mice with improved efficiency. Bioelectromagnetics. 37: 223-233.

Collin A, Perrin A, Cretallaz C, Pla S, Arnaud-Cormos D, Debouzy JC, Leveque P. 2016. In vivo setup characterization for pulsed electromagnetic field exposure at 3 GHz. Phys Med Biol. 61: 5925-5941.

Grigoriev YG, Grigoriev OA, Ivanov AA, Lyaginskaya AM, Merkulov AV, Shagina NB, Maltsev VN, Lévêque P, Ulanova AM, Osipov VA, Shafirkin AV. 2010. Confirmation

studies of Soviet research on immunological effects of microwaves: Russian immunology results. Bioelectromagnetics. 31(8):589–602.

Poulletier de Gannes F, Taxile M, Duleu S, Hurtier A, Haro E, Geffard M, Ruffié G, Billaudel B, Lévêque P, Dufour P, Lagroye I, Veyret B. 2009. A confirmation study of Russian and Ukrainian data on effects of 2450 MHz microwave exposure on immunological processes and teratology in rats. Radiation Research. 172(5):617–24.

Costa FP, de Oliveira AC, Meirelles R, Machado MC, Zanesco T, Surjan R, Chammas MC, de Souza Rocha M, Morgan D, Cantor A, Zimmerman J, Brezovich I, Kuster N, Barbault A, Pasche B. 2011. Treatment of advanced hepatocellular carcinoma with very low levels of amplitude-modulated electromagnetic fields. Br J Cancer. 105: 640-648.

Gabriel S, Lau RW, and Gabriel C. 1996. The dielectric properties of biological tissues: II. Measurements in the in the frequency range 10 Hz to 20 GHz. Physics in medicine and biology. 41(11):2251-69.

Jimenez H, Blackman C, Lesser G, Debinski W, Chan M, Sharma S, Watabe K, Lo HW, Thomas A, Godwin D, Blackstock W, Mudry A, Posey J, O'Connor R, Brezovich I, Bonin K, Kim-Shapiro D, Barbault A, Pasche B. 2018. Use of non-ionizing electromagnetic fields for the treatment of cancer. Frontiers in bioscience (Landmark edition). 23: 284-297.

Jimenez H, Wang M, Zimmerman JW, Pennison MJ, Sharma S, Surratt T, Xu ZX, Brezovich I, Absher D, Myers RM, DeYoung B, Caudell DL, Chen D, Lo HW, Lin HK, Godwin DW, Olivier M, Ghanekar A, Chen K, Miller LD, Gong Y, Capstick M, D'Agostino RB, Munden R, Merle P, Barbault A, Blackstock AW, Bonkovsky HL, Yang GY, Jin G, Liu L, Zhang W, Watabe K, Blackman CF, Pasche BC. 2019. Tumour-specific amplitude-modulated radiofrequency electromagnetic fields induce differentiation of hepatocellular

carcinoma via targeting Cav3.2 T-type voltage-gated calcium channels and Ca2+influx. EBioMedicine. 44: 209-224.

Leveque P, Reineix A, Jecko B. 1992. Modelling of dielectric losses in microstrip patch antennas: application of FDTD method Electronics letters. 28: 539-541.

Sharma S, Wu SY, Jimenez H, Xing F, Zhu D, Liu Y, Wu K, Tyagi A, Zhao D, Lo HW, Metheny-Barlow L, Sun P, Bourland JD, Chan MD, Thomas A, Barbault A, D'Agostino RB, Whitlow CT, Kirchner V, Blackman C, Pasche B, Watabe K. 2019. Ca2+and CACNA1H mediate targeted suppression of breast cancer brain metastasis by AM RF EMF. EBioMedicine. 44: 194-208.

Taflove A, Hagness SC. 2005. *Computational Electrodynamics: The Finite-difference Time-domain Method*. Artech House

Tuttle RR, Mills J. 1975. Dobutamine: development of a new catecholamine to selectively increase cardiac contractility. Circ Res. 36: 185-196.

Wu T, Hadjem A, Wong MF, Gati A, Picon O, Wiart J. 2010. Whole-body new-born and young rats' exposure assessment in a reverberating Physics in medicine and biology. 55: 1619-1630.

Yee K.1966. Numerical solution of initial boundary value problems involving maxwell's equations in isotropic media IEEE Transactions on Antennas and Propagation. 14: 302-307.

Zimmerman JW, Jimenez H, Pennison MJ, Brezovich I, Morgan D, Mudry A, Costa FP, Barbault A, Pasche B. 2013. Targeted treatment of cancer with radiofrequency electromagnetic fields Chinese journal of cancer. 32: 573-581.

Zimmerman JW, Pennison MJ, Brezovich I, Yi N, Yang CT, Ramaker R, Absher D, Myers RM, Kuster N, Costa FP, Barbault A, Pasche B. 2012. Cancer cell proliferation is inhibited by specific modulation frequencies. Br J Cancer. 106: 307-313.

		HuH7 tumor size (mm^3)			HepG2 tumor size (mm^3)		
		≤50	**51-200**	**>200**	**≤50**	**51-200**	**>200**
Frequency Range Scanned	1-400 Hz	n.d.	n.d.	2	1	2	n.d.
	2300-2700 Hz	1	4	3	3	2	n.d.
	4000-4400 Hz	n.d.	2	2	2	n.d.	n.d.
	10 kHz-10.5 kHz	n.d.	2	n.d.	2	n.d.	n.d.
	100-100.4 kHz	2	1	n.d.	n.d.	n.d.	n.d.
HCC-specific frequencies	410.231Hz to 2419.309 Hz	n.d.	5	2	5	4	n.d.
	4289.296 Hz to 6733.331 Hz	1	2	1	1	1	n.d.

Table 1: Number of replicates performed with mice bearing HuH7 or HepG2 xenografted tumors of the indicated size and exposed to the indicated amplitude-modulated frequencies. n.d.: not determined.

Figure legends

Figure 1: Experimental setup used to search for effects of AM-RF on pulse oxymetry in freely-moving awake mice. Mice plethysmographic waveforms were recorded on freely-moving awake mouse fitted with a proprietary pulse oximeter, the CollarClip sensor of which was placed on the shaved skin on the mice necks and exposed to the AM-RF. An in-house LabView software was developed to acquire and analyze the raw pulse signals recorded through an A/D converter data acquisition card. The exposure setup was composed of a low-frequency (LF) generator modulating a high-frequency (HF) RF generator emitting a 27.12 MHz carrier wave, a directional coupler which allowed forward and reflected signal

measurement, and a 50 Ω impedance matching device maximizing power transfer into the mouse through a disposable electrode stuck to the mouse shaved neck.

Figure 2: Setup for electromagnetic characterization. A) Setup for the experimental electrical analysis and for the impedance monitoring using the matching box; The exposure setup was composed of a 27 MHz signal generator, a directional coupler for forward and reflected signal measurement using an oscilloscope, and a 50 ohms impedance matching device maximizing power transfer into the sample; (B) 3D view of the simulated setup for performing impedance and SAR dosimetry. A coaxial cable with inner and outer conductors connected to the exposed sample and to the ground plane. The animal was insulated from the ground plane by a plastic layer.

Figure 3: Electrical characterization. A) S_{11} reflection coefficient of the delivery system (mouse, plastic layer, electrode, BNC connector, coaxial cable) using the matching device with C1=47.8 pF, C2=179 pF, and L=0.7 μH; the red dotted line highlights the 27 MHz frequency; B) Normalized spatial SAR distribution (dB) at 27 MHz, with a uniform 0.33 x 0.33 x 0.33 mm mesh grid. The SAR on the animal skin is represented.

Figure 4. Effect of intraperitoneal injection of Dobutamine on mice pulse signal. Pulse oximetry signal from an anesthetized RAG-2/γ(c)KO mouse was recorded in real time before and after IP injection of Dobutamine A) Mouse pulse amplitude and frequency were recorded before and after intraperitoneal injection of Dobutamine. B) Ten-second extract of mouse pulse pleth signal recorded before (upper panel) and after (lower panel) IP injection of Dobutamine in anesthetized mice.

Figure 5: Effect of HCC-specific amplitude-modulated frequencies on mice pulse amplitude and frequency. Freely-moving awake mice were sequentially sham exposed or RF exposed to HCC-specific frequencies (as indicated in the upper panel) while mice pulse amplitude (middle panel) and pulse frequency (lower panel) were recorded in real-time. The

graphs, recorded during the scan of HCC frequencies ranging from 410.231 Hz and 2419.309 Hz using a mouse xenografted with HuH7 cells leading a tumor of 75 mm^3 the day of the experiment, are representatives of the results obtained with any of the 22 recording sessions performed using two different sets of HCC-specific modulation frequencies, two different HCC xenografted mouse models and various tumor volumes up to 1000 mm^3 (see Table 1 for exposure conditions details).

Figure 6: Average amplitude of mice pulses during scans of AM frequencies. The average amplitude of mice pulses was monitored in real-time while freely-moving awakens mice bearing xenografted tumors were exposed at frequencies ranging from 2300 Hz to 2700 Hz using a 2 Hz step (A) or sham-exposed (B). The mice's pulse response under exposure to each modulation frequency was recorded for 4 s and averaged over this time period. Each trace represents one of the experimental conditions indicated in Table 1 for the 2300-2700 Hz range. The figure is representative of the mice's pulse response in the other scanned AM-frequencies ranges that are indicated in Table 1.

Figure 7: Peak-to-peak analysis of mice oxymetry pulses amplitude during scans of AM-RF frequencies between 2300 and 2700 Hz. A) Schematic representation of the analysis performed. For each AM frequency tested, the average amplitude $\bar{X}$ of the mice pulses over the 4 s recording period, along with the related standard deviation (σ) was calculated. Then the percentage of beats for which the peak-to-peak amplitude or frequency exceeded $\bar{X}+2\sigma$ was calculated. B) Percentage of pulses exceeding the confidence interval (set to 2 times the standard deviation). The reported data were averaged over all experimental conditions tested in terms of tumor size and xenograft type using AM-RF in the 2300-2700 MHz range (see table 1).

Supplementary figure 1: Effect of mice movement on mice pulse amplitude and frequency signals. Mouse pulse frequency and pulse amplitude were recorded once per

second. Red inset shows a mouse pulse pleth signal when a movement was detected. Black inset shows a mouse pulse pleth signal when no movement was detected.

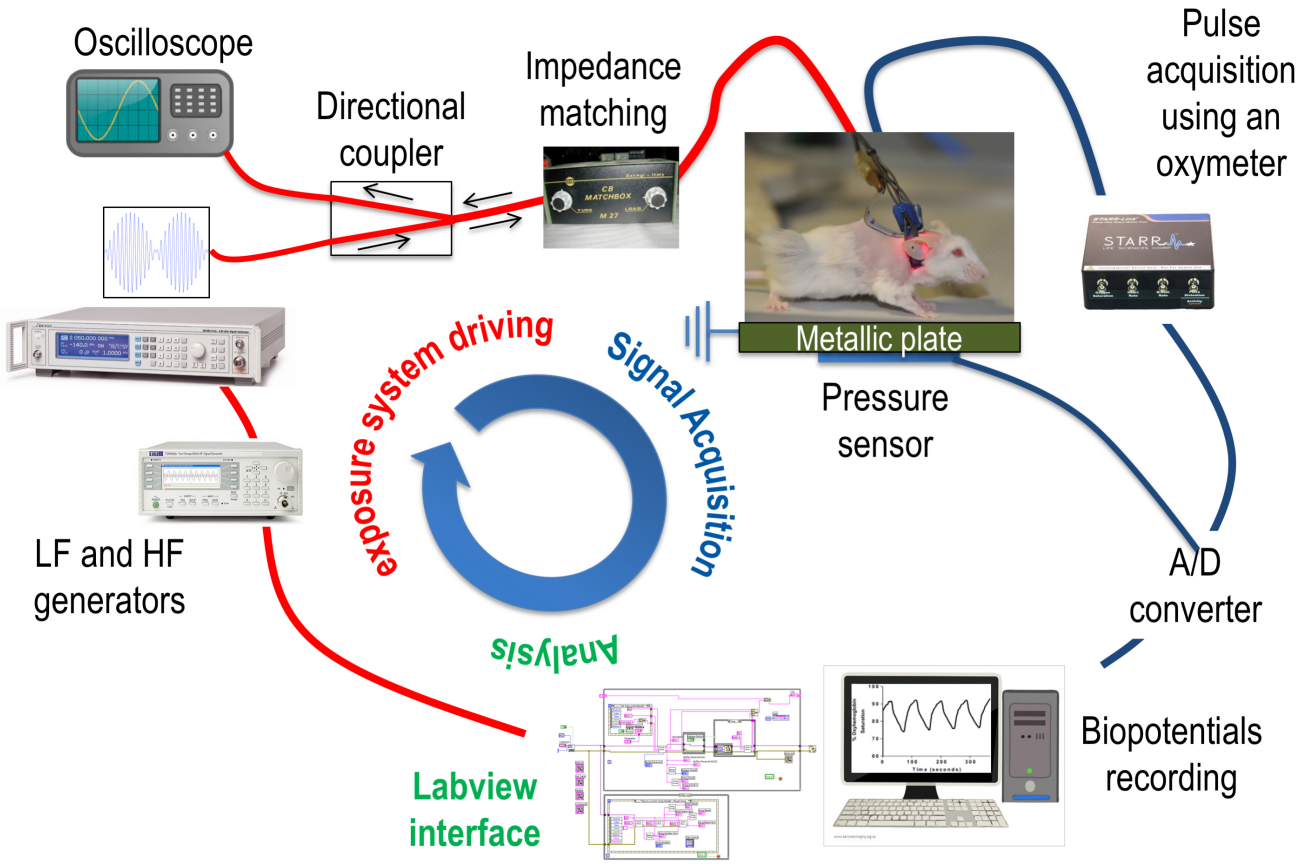
Oscilloscope
Directional coupler
Impedance matching
Pulse acquisition using an oxymeter
Metallic plate
Pressure sensor
LF and HF generators
exposure system driving
Signal Acquisition
Analysis
A/D converter
Labview interface
Biopotentials recording

Figure 1

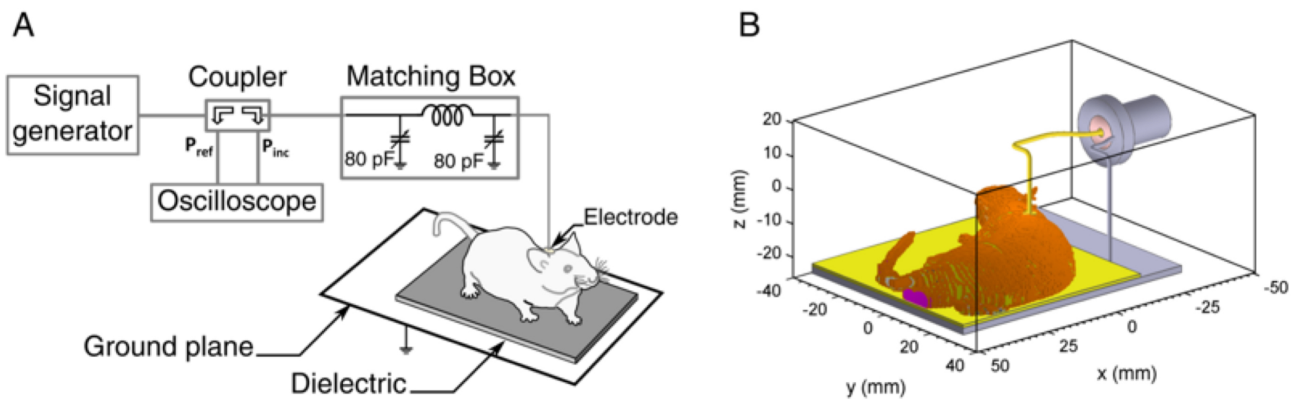
A
Signal generator
Coupler
Matching Box
P_{ref}
P_{inc}
80 pF
80 pF
Oscilloscope
Electrode
Ground plane
Dielectric
B
z (mm)
20
10
0
-10
-20
-40
-20
0
20
40
y (mm)
50
25
0
-25
-50
x (mm)

Figure 2

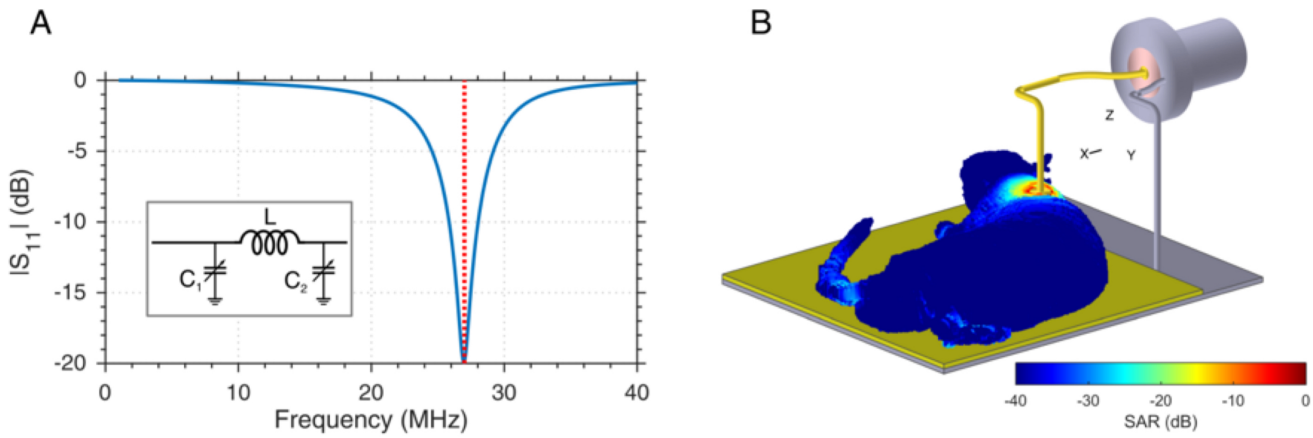
A
0
-5
-10
-15
-20
|S11| (dB)
0
10
20
30
40
Frequency (MHz)
L
C1
C2
B
Z
X
Y
-40
-30
-20
-10
0
SAR (dB)

Figure 3

A

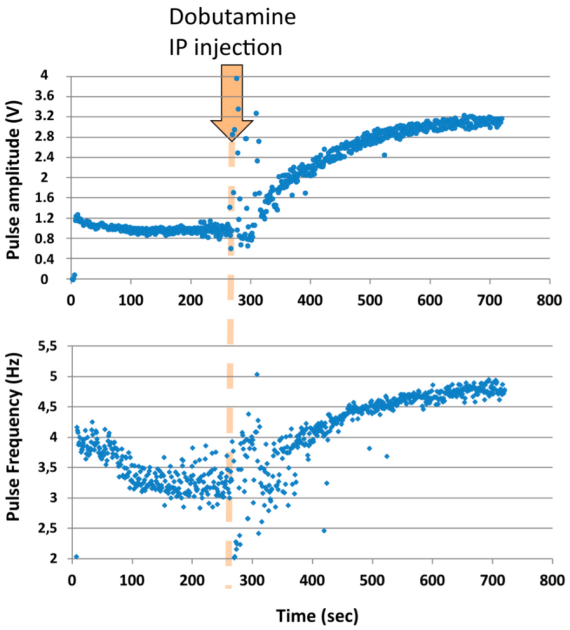
Dobutamine
IP injection
Pulse amplitude (V)
Pulse Frequency (Hz)
Time (sec)

B

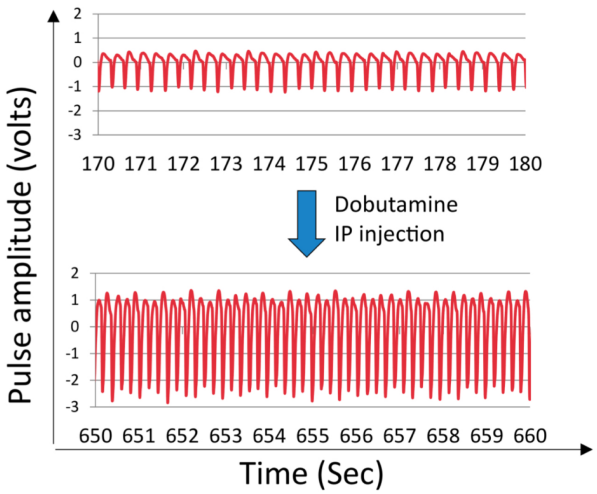
Pulse amplitude (volts)
Dobutamine
IP injection
Time (Sec)

Figure 4

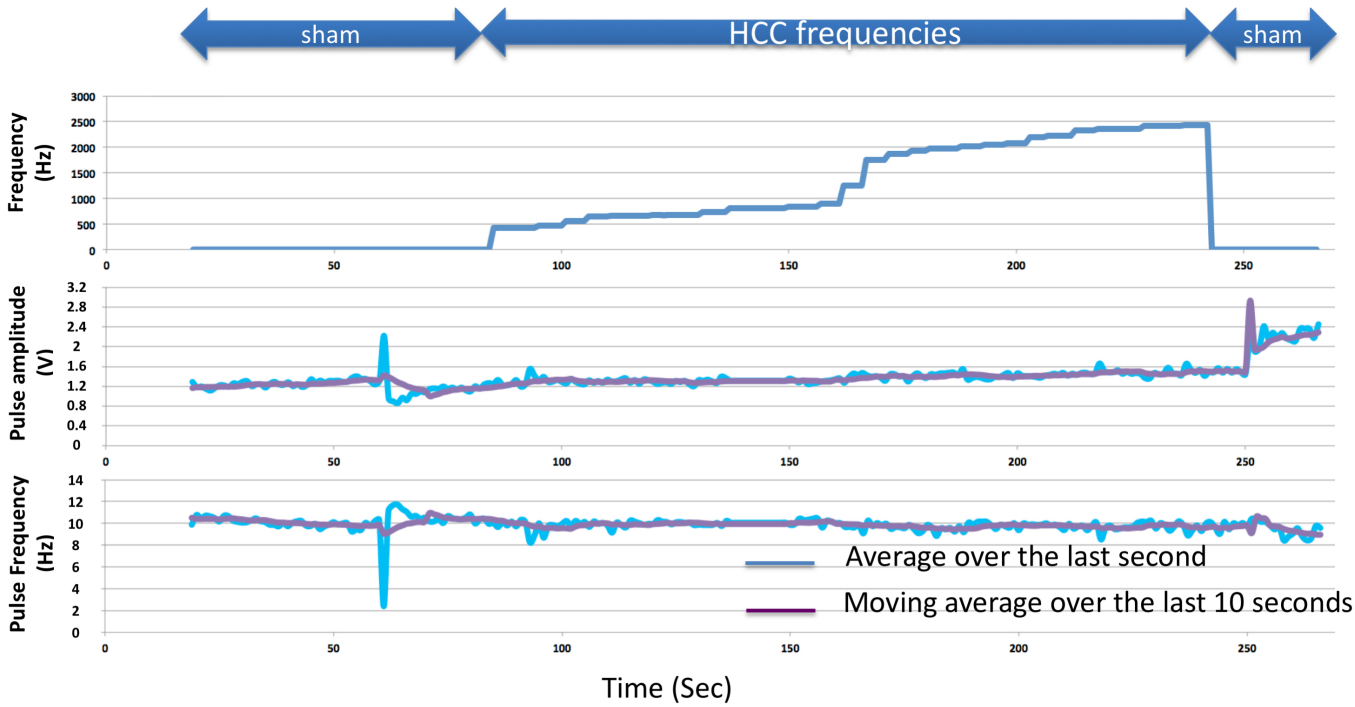
sham
HCC frequencies
sham
Frequency (Hz)
3000
2500
2000
1500
1000
500
0
Pulse amplitude (V)
3.2
2.8
2.4
2
1.6
1.2
0.8
0.4
0
Pulse Frequency (Hz)
14
12
10
8
6
4
2
0
0
50
100
150
200
250
Average over the last second
Moving average over the last 10 seconds
Time (Sec)

Figure 5

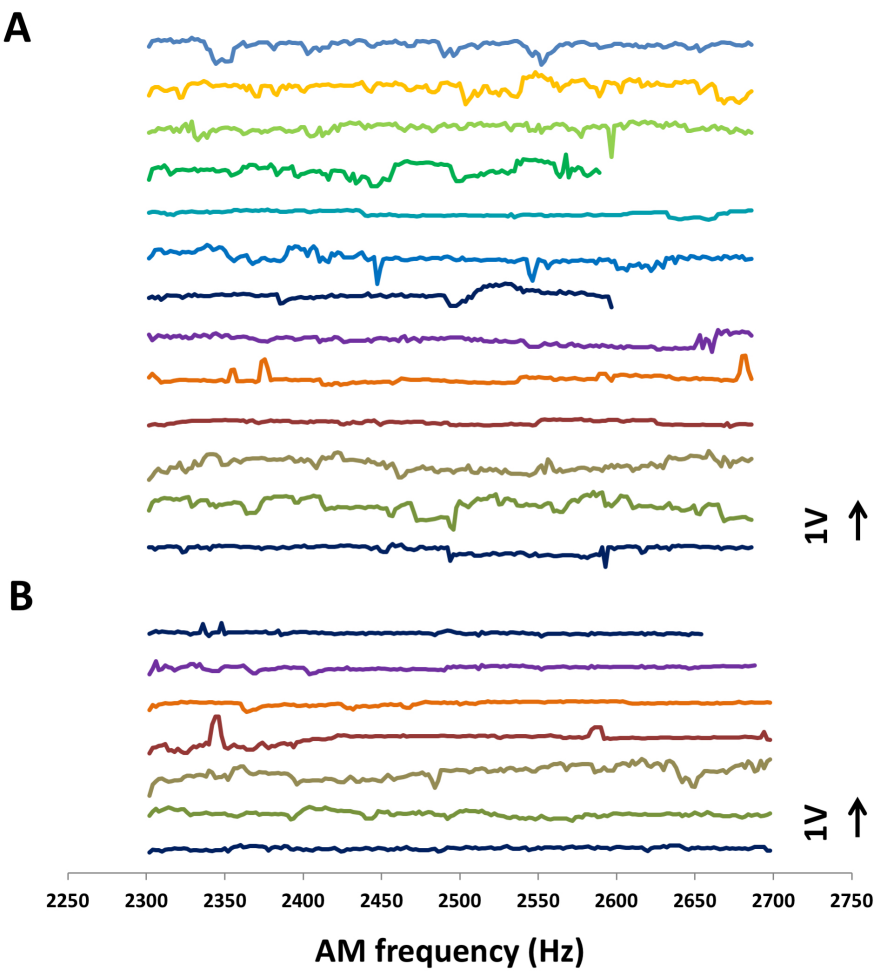
A
B
1V
1V
2250
2300
2350
2400
2450
2500
2550
2600
2650
2700
2750
AM frequency (Hz)

Figure 6

A

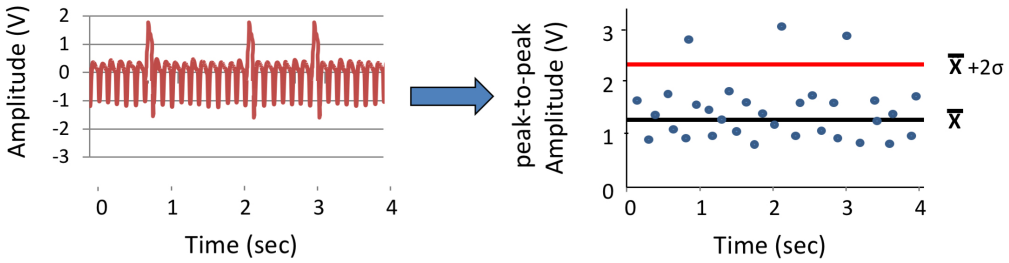
Amplitude (V)
2
1
0
-1
-2
-3
0
1
2
3
4
Time (sec)
peak-to-peak Amplitude (V)
3
2
1
0
0
1
2
3
4
Time (sec)
$\bar{x}$ +2σ
$\bar{x}$

B

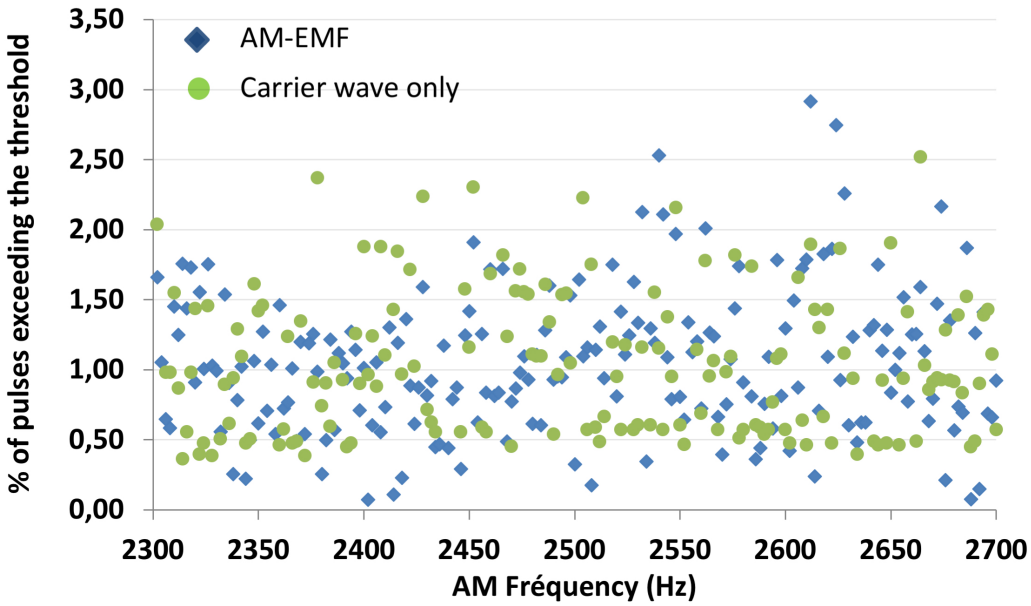
% of pulses exceeding the threshold
3,50
3,00
2,50
2,00
1,50
1,00
0,50
0,00
AM-EMF
Carrier wave only
2300
2350
2400
2450
2500
2550
2600
2650
2700
AM Fréquency (Hz)

Figure 7

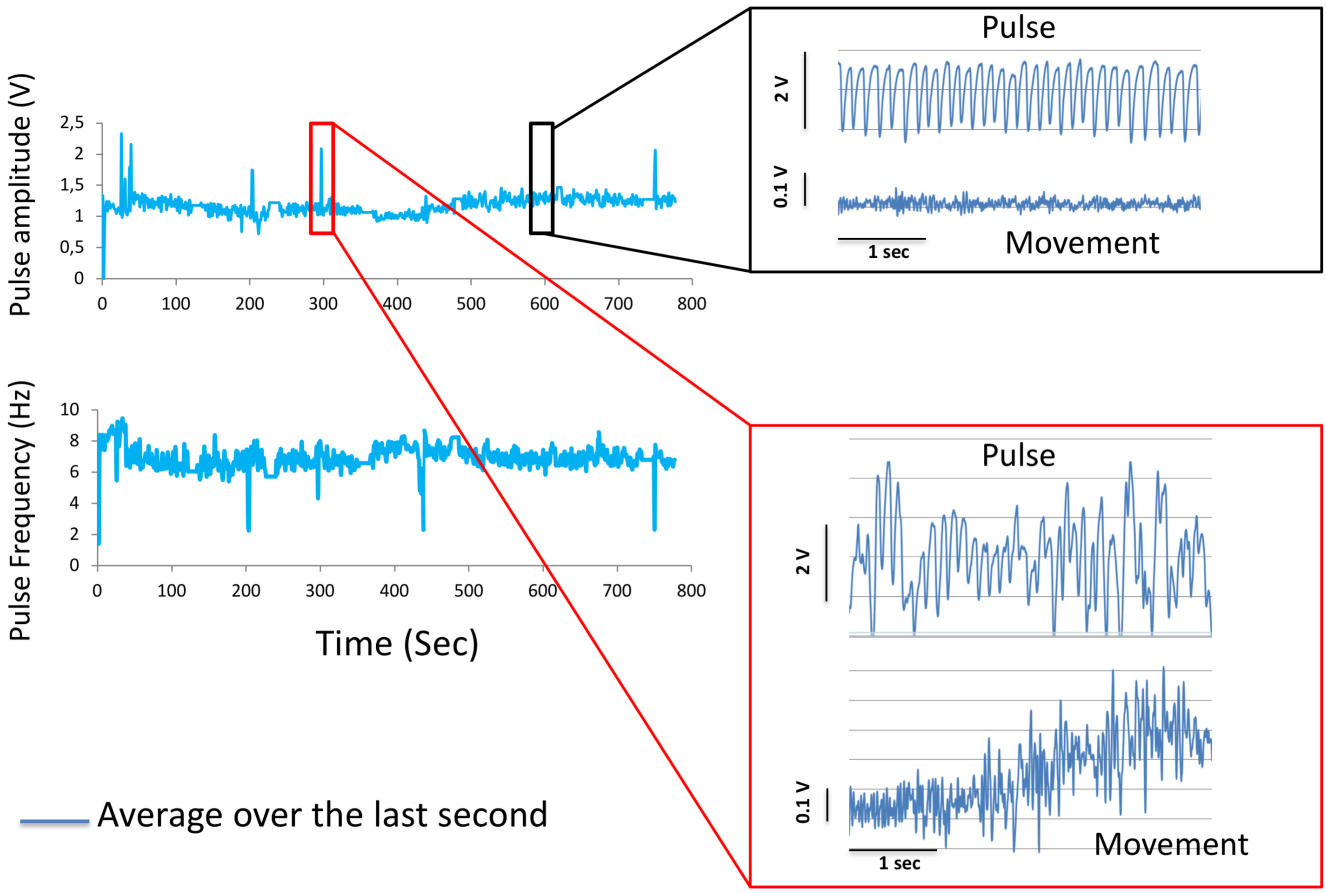

Supplementary Figure 1